
UNDERSTANDING MEMORIZATION IN GENERATIVE MODELS VIA SHARPNESS IN PROBABILITY LANDSCAPES

Dongjae Jeon
Yonsei University
dongjae0324@yonsei.ac.kr

Dueun Kim
Yonsei University
jinha2536@yonsei.ac.kr

Albert No
Yonsei University
albertno@yonsei.ac.kr

ABSTRACT

In this paper, we introduce a geometric framework to analyze memorization in diffusion models using the eigenvalues of the Hessian of the log probability density. We propose that memorization arises from isolated points in the learned probability distribution, characterized by sharpness in the probability landscape, as indicated by large negative eigenvalues of the Hessian. Through experiments on various datasets, we demonstrate that these eigenvalues effectively detect and quantify memorization. Our approach provides a clear understanding of memorization in diffusion models and lays the groundwork for developing strategies to ensure secure and reliable generative models.

1 Introduction

Recent advancements in generative models have revolutionized data generation tasks across diverse domains, including image synthesis [Rombach et al., 2022], natural language processing [Achiam et al., 2023, Touvron et al., 2023], video generating [Ho et al., 2022, Brooks et al., 2022], and molecular design [Alakhdar et al., 2024]. Among these, diffusion models have emerged as a particularly powerful framework, capable of producing high-quality and diverse outputs. Diffusion models [Ho et al., 2020, Song et al., 2021a] work by learning to reverse a predefined noise-adding diffusion process. Their ability to approximate complex data distributions through iterative denoising has achieved state-of-the-art results in applications ranging from image generation [Song et al., 2021b, Saharia et al., 2022] to text-to-image tasks [Rombach et al., 2022, Podell et al., 2024].

Despite their successes, diffusion models face challenges such as overfitting and memorization [Carlini et al., 2023, Somepalli et al., 2023b, Webster, 2023], where models replicate training data rather than generalizing to new inputs. Memorization is especially problematic in scenarios involving sensitive data, as it risks privacy violations [Orrick, 2023, Joseph Saveri, 2023] and undermines model robustness. Addressing memorization is therefore critical for deploying diffusion models in trustworthy and secure settings.

There has been substantial prior work aimed at understanding memorization in diffusion models, which has contributed to a broader understanding of this phenomenon in generative models [Carlini et al., 2023, Somepalli et al., 2023a]. Existing approaches include analyzing probability manifolds using Local Intrinsic Dimensionality (LID) [Ross et al., 2024, Kamkari et al., 2024], leveraging spectral properties to characterize memorization [Ventura et al., 2024, Stanczuk et al., 2024], and employing score-based techniques to measure discrepancies between conditional and marginal scores [Wen et al., 2024]. Additionally, recent studies have explored cross-attention mechanisms to detect and analyze memorization [Ren et al., 2024, Chen et al., 2024].

In this work, we introduce a theoretical framework to characterize memorization in diffusion models through the lens of geometric analysis. We propose that memorization arises from isolated points in the learned probability distribution, which manifest as regions of *sharpness* in the probability landscape. This sharpness can be effectively identified by analyzing the eigenvalues of the Hessian of the log probability. Our approach provides a principled framework rooted in the geometry of the learned probability distribution, offering both interpretability and a solid theoretical foundation.

By analyzing the Hessian of the log probability and its eigenvalues, which correspond to the Jacobian of the score function, we develop a diagnostic tool to identify memorization. Our framework reveals that large negative eigenvalues of the Hessian serve as a reliable indicator of memorization, signaling the presence of isolated points in the learned distribution. Moreover, by inspecting the number of positive eigenvalues, we quantify the degree of memorization, enabling distinctions between categories such as template verbatim and matching verbatim memorization. This

perspective also sheds light on how memorization reduces the effective degrees of freedom in the model’s learned distribution, ultimately constraining its ability to generalize.

Hessian eigenvalue computation, however, is not straightforward and presents significant challenges, particularly in high-dimensional settings. To address this, we take two approaches: learning the second-order score function Lu et al. [2022], Meng et al. [2021], which directly computes the Hessian of the log probability, and using Arnoldi iteration Arnoldi [1951] for eigenvalue estimation, which is particularly well-suited for large-scale applications such as Stable Diffusion Rombach et al. [2022].

We also present extensive experimental results to validate our theoretical findings. Our experiments, conducted on a toy 2D dataset, MNIST, and Stable Diffusion, consistently demonstrate that regions of memorization are characterized by significant negative eigenvalues of the Hessian. Additionally, the degree of memorization, quantified through the number of positive eigenvalues, offers a robust metric for assessing its extent and categorizing its nature. These results provide strong empirical support for our geometric framework, advancing the understanding of memorization in diffusion models and establishing practical tools for its reliable detection and analysis.

The primary contributions of this paper are as follows:

- We introduce a geometric perspective on memorization in diffusion models, highlighting the role of sharpness in the probability landscape.
- We propose counting the strictly positive eigenvalues of the Hessian of the log probability (or equivalently, the Jacobian of the score function) as a metric to detect and quantify memorization.
- Extensive experiments on 2D toy datasets, MNIST, and Stable Diffusion validate the effectiveness of our method in identifying memorization with high precision, bridging theoretical insights and practical applications.

2 Related works

Understanding and Explaining Memorization Several studies [Somepalli et al., 2023b, Carlini et al., 2023, Wen et al., 2024] have investigated the memorization behavior of diffusion models (DMs), focusing primarily on factors such as prompts [Somepalli et al., 2023a], data duplication [Carlini et al., 2023, Somepalli et al., 2023b], and the size or complexity of the training data [Somepalli et al., 2023b]. Some works analyze this phenomenon from a geometric perspective, grounded in the widely accepted manifold learning conjecture that high-dimensional data resides on a relatively low-dimensional latent manifold [Fefferman et al., 2016, Pope et al., 2021], with exact memorization corresponding to a zero-dimensional manifold [Ross et al., 2024, Ventura et al., 2024, Pidstrigach, 2022]. This perspective has motivated several approaches for estimating the Local Intrinsic Dimensionality (LID) of individual data points [Stanczuk et al., 2024, Kamkari et al., 2024, Horvat and Pfister, 2024, Wenliang and Moran, 2023, Tempczyk et al., 2022], which are then employed to explain memorization phenomena [Ross et al., 2024, Ventura et al., 2024].

Although our work aligns with some conclusions from previous studies, it differs in important ways. Unlike Yoon et al. [2023], Gu et al. [2023], which define memorization globally at the model level, our approach adopts a geometric perspective focused on local data points, aligning more closely with Ross et al. [2024], Bhattacharjee et al. [2023], Ventura et al. [2024]. However, in contrast to Ross et al. [2024], Bhattacharjee et al. [2023], which rely on ground truth density to define memorization, or Ventura et al. [2024], which examines the interplay between memorization and generalization, we make no assumptions about data densities and do not explicitly address generalization. Instead, we define memorization solely in terms of the local “sharpness” of the learned density.

Additionally, when explaining LID, our method avoids the limitations of existing LID estimators. For instance, FLIPD [Kamkari et al., 2024] is sensitive to network architecture and unstable near $t \rightarrow 0$, where learned scores often diverge, while the Normal Bundle (NB) estimator [Stanczuk et al., 2024] incurs substantial computational costs in high-dimensional settings. By directly analyzing the Jacobian of the learned scores (equivalent to the Hessian of the log density), our approach eliminates parameter dependencies and avoids additional network training, consistently delivering accurate LID estimates across timesteps. Furthermore, it scales effectively to high-dimensional scenarios, such as those in Stable Diffusion, by leveraging Arnoldi iteration and `torch.autograd.jvp` for computational efficiency.

While our work focuses exclusively on understanding the memorization phenomenon in diffusion models (DMs), it is inherently connected to the broader topic of generalization. Several studies have explored how DMs generalize, offering insights that complement our findings on memorization. Kadkhodaie et al. [2024] highlight that DMs possess an inductive bias that aids generalization, while Yi et al. [2023] attribute this ability to an optimization bias. Furthermore, Yoon et al. [2023] demonstrate a trade-off between memorization and generalization, showing that DMs tend to generalize more effectively when their capacity for memorization is constrained. These studies underscore

the interconnected nature of memorization and generalization, situating our work within a broader framework of understanding diffusion models.

Detecting Memorization Detecting memorization in generated content remains a challenging and unresolved problem. Recent studies have proposed various methods to extract memorized samples from diffusion models. For example, Somepalli et al. [2023a] utilized detectors like SSCD [Pizzi et al., 2022] and DINO [Caron et al., 2021] to identify memorized samples. Carlini et al. [2023] introduced calibrated ℓ_2 distance in pixel space to compare generated images against training data, an approach also adopted by Yoon et al. [2023] and Stein et al. [2023]. Moreover, Webster [2023] developed white-box and black-box attacks, focusing on edges and noise in generated images to detect memorization.

While these methods have advanced the field, they remain computationally intensive, limiting their feasibility for broader applications. To address these limitations, alternative detection strategies have been explored. For instance, Wen et al. [2024] proposed analyzing differences between text-conditioned and unconditioned score predictions to identify memorized prompts. Ren et al. [2024] demonstrated that unusually high cross-attention scores for specific tokens are strong indicators of memorization. Similarly, Chen et al. [2024] examined end tokens of text embeddings to uncover memorized content.

3 Preliminaries

Score-based Diffusion Models. The foundation of diffusion models (DMs), widely used for image generation, lies in score-based models [Song et al., 2021c]. These models corrupt the given training data which follows $p_0(\mathbf{x}_0)$ by adding random noise and then learn the score function, the gradient of the log density, $\nabla_{\mathbf{x}} \log p_t(\mathbf{x}_t)$. Subsequently, a reverse process is applied to generate new samples, starting from arbitrary noise, which follow the same distribution as the original data.

We define forward process and corresponding reverse process as

$$d\mathbf{x}_t = f(\mathbf{x}_t, t)dt + g(t)d\mathbf{w}_t$$

and

$$d\bar{\mathbf{x}}_t = (f(\bar{\mathbf{x}}_t, t) - g^2(t)\nabla_{\mathbf{x}_t} \log p_t(\bar{\mathbf{x}}_t)) dt + g(t)d\bar{\mathbf{w}}_t,$$

where \mathbf{w}_t and $\bar{\mathbf{w}}_t$ are forward and reverse-time standard Brownian motion.

Since we cannot access to score function, we parametrize it with $s_\theta(x, t)$ through neural network. Optimizing the score matching loss

$$\mathcal{L}_{SM}(\theta) = \int_0^T \lambda(t) \mathbb{E}_{\mathbf{x}_t} \left[\|s_\theta(\mathbf{x}_t, t) - \nabla_{\mathbf{x}_t} \log p_t(\mathbf{x}_t)\|^2 \right] dt$$

is intractable as we do not have actual score function, so we use alternative(equivalent) formula. Let us discretize the forward process as $\mathbf{x}_t | x_0 \sim \mathcal{N}(\alpha_t \mathbf{x}_0, \sigma_t^2 \mathbf{I})$ for $\alpha_t \in \mathbb{R}$, $\sigma_t \in \mathbb{R}_{++}$. For a fixed time point t , we can define

$$\theta^* = \arg \min_{\theta} \mathbb{E}_{\mathbf{x}_0, \epsilon} \left[\frac{1}{\sigma_t^2} \|\sigma_t s_\theta(\mathbf{x}_t, t) + \epsilon\|_2^2 \right], \quad \mathbf{x}_t = \alpha_t \mathbf{x}_0 + \sigma_t \epsilon, \quad \epsilon \sim \mathcal{N}(\mathbf{0}, \mathbf{I}),$$

which is called denoising score matching(DSM). Practically, we can use Monte Carlo method to approximate integral over t .

Sharpness and Hessian. For a given function f at a point x , the Hessian $\nabla_x^2 f(x)$ encapsulates the second-order derivatives, providing a representation of the local curvature of f around x . The eigenvectors of the Hessian define the principal axes of this curvature, which are often orthogonal, while the corresponding eigenvalues quantitatively describe the curvature along these directions. Positive eigenvalues indicate directions of local convexity, negative eigenvalues denote directions of local concavity, and zero eigenvalues correspond to flat regions. The magnitude of an eigenvalue reflects the steepness of the curvature, with larger absolute values indicating more pronounced variations. Thereby, by examining the eigenvalues of the Hessian at a specific point, we gain insights into the structure and geometry of the landscape at that point. In this paper, we primarily focus on the Hessian of the log density, which can also be interpreted as the Jacobian of the score function. Throughout the paper, we denote the Hessian of the log density as $H(\mathbf{x}_t, t) := \nabla_{\mathbf{x}_t}^2 \log p_t(\mathbf{x}_t)$ for the unconditional case and $H(\mathbf{x}_t, t, c) := \nabla_{\mathbf{x}_t}^2 \log p_t(\mathbf{x}_t | c)$ for the conditional case.

Second Order Score Function Since the Hessian of interest is simply the Jacobian of the score function, it can be directly computed using automatic differentiation from a trained DM. While a well-trained DM that accurately estimates scores should theoretically yield an accurate Hessian via automatic differentiation, this is not always the case in practice. Therefore, to achieve a more accurate estimation of the Hessian, the model should be parameterized and incorporate a second-order score matching loss that estimates $\nabla_{\mathbf{x}_t}^2 \log p_t(\mathbf{x}_t) \approx \nabla_{\mathbf{x}_t} s_\theta(\mathbf{x}_t, t) := s_\theta^{(2)}(\mathbf{x}_t, t)$ as demonstrated by Meng et al. [2021]. This can be interpreted as implicit ‘‘correction’’ of the parametrized score function. To enhance numerical stability in the loss function, we adopt the loss proposed by Lu et al. [2022], an improved version of the loss utilized by Meng et al. [2021]. For a fixed t and given trained score function, this loss is defined as

$$\theta^* = \arg \min_{\theta} \mathbb{E}_{\mathbf{x}_0, \epsilon} \left[\frac{1}{\sigma_t^4} \left\| \sigma_t^2 s_\theta^{(2)}(\mathbf{x}_t, t) + \mathbf{I} - \ell_1 \ell_1^\top \right\|_F^2 \right],$$

where $\ell_1(\epsilon, \mathbf{x}_0, t) := \sigma_t s_\theta(\mathbf{x}_t, t) + \epsilon$, $\mathbf{x}_t = \alpha_t \mathbf{x}_0 + \sigma_t \epsilon$, $\epsilon \sim \mathcal{N}(\mathbf{0}, \mathbf{I})$. The proposed objective is

$$\mathcal{L}_{DSM}^{(2)}(\theta) := \mathbb{E}_{t, \mathbf{x}_0, \epsilon} \left[\left\| \sigma_t^2 s_\theta^{(2)}(\mathbf{x}_t, t) + \mathbf{I} - \ell_1 \ell_1^\top \right\|_F^2 \right].$$

Numerical Eigenvalue Algorithms For high-resolution image data with very large dimensions, such as in Stable Diffusion, calculating the exact Hessian and finding its eigenvalues are computationally complex and memory inefficient. As an alternative, we employ Arnoldi iteration [Arnoldi, 1951], a numerical algorithm that leverages the efficient computation of Hessian-vector products via `torch.autograd.functional.jvp` to approximate some leading eigenvalues without forming the Hessian explicitly. In more detail, we can compute the action of the Hessian on a vector \mathbf{v} efficiently using automatic differentiation. Arnoldi iteration is an algorithm derived from the Krylov subspace method that constructs an orthonormal basis $\mathbf{Q}_m = [\mathbf{q}_1, \mathbf{q}_2, \dots, \mathbf{q}_m]$ of the Krylov subspace K_m , and an upper Hessenberg matrix \mathbf{H}_m , such that the following relationship holds:

$$\mathbf{A}\mathbf{Q}_m = \mathbf{Q}_m\mathbf{H}_m + h_{m+1,m}\mathbf{q}_{m+1}\mathbf{e}_m^\top,$$

where \mathbf{e}_m is the m -th canonical basis vector. Since we can compute $\mathbf{A}\mathbf{q}_k$ without forming \mathbf{A} explicitly, using the function `jvp_func(qk)`, the Arnoldi iteration proceeds as follows. First, we normalize the starting vector \mathbf{b} to obtain $\mathbf{q}_1 = \frac{\mathbf{b}}{\|\mathbf{b}\|_2}$. Then, for each iteration $k = 1$ to m , we compute:

$$\mathbf{v} = \text{jvp_func}(\mathbf{q}_k),$$

which represents the action of \mathbf{A} on \mathbf{q}_k . We then orthogonalize \mathbf{v} against the previous basis vectors $\mathbf{q}_1, \dots, \mathbf{q}_k$, updating \mathbf{h} and \mathbf{v} :

$$h_{j,k} = \mathbf{q}_j^\top \mathbf{v}, \quad \mathbf{v} = \mathbf{v} - h_{j,k} \mathbf{q}_j, \quad \text{for } j = 1, \dots, k.$$

After orthogonalization, we compute $h_{k+1,k} = \|\mathbf{v}\|_2$. If $h_{k+1,k}$ is greater than a small threshold ϵ , we normalize \mathbf{v} to obtain the next basis vector $\mathbf{q}_{k+1} = \frac{\mathbf{v}}{h_{k+1,k}}$. Otherwise, the iteration terminates. The eigenvalues of \mathbf{H}_m (Ritz values) approximate the m eigenvalues of \mathbf{A} . For details on the computational process of Arnoldi iteration, please refer to Appendix B.

The Arnoldi iteration tends to find eigenvalues with larger absolute values first because components associated with these eigenvalues dominate within the Krylov subspace. If the input matrix is symmetric, Arnoldi iteration can be simplified to Lanczos iteration [Lanczos, 1950]. However, since the Lanczos iteration is very sensitive to small numerical errors breaking the symmetry, we use the general version. The computational complexity of the algorithm is $O(m^2d)$ with space complexity $O(md)$, compared to $O(d^3)$ with $O(d^2)$ of exact derivation and eigendecomposition of Hessian. We calculate all eigenvalues for several samples for clear justification. But with just a few ($m \ll d$) iterations, the difference between memorized samples and non-memorized samples reveals enough.

4 Understanding Memorization in Geometric Perspective

4.1 Sharpness in Probability Landscape and Memorization

Memorization in diffusion models refers to the phenomenon where the learned data distribution becomes excessively concentrated at isolated points, typically corresponding to the training data. This occurs when the model overfits, effectively collapsing the learned probability distribution into individual samples. Biroli et al. [2024] describe this phenomenon in terms of phase transitions in the sampling path, which lead to such localized distributions.

In the sampling process, the score function guides the steepest ascent of the log-likelihood in the data space, analogous to gradient ascent [Das, 2024]. In deterministic scenarios, the sampling process converges to local modes of the target distribution. However, the addition of noise during the sampling process allows the model to explore broader regions of the data space. When memorization occurs, this broader exploration is compromised, and the learned density exhibits sharp, localized peaks centered on training samples.

We hypothesize that memorization can be characterized by the sharpness of the probability landscape, where sharpness corresponds to steep gradients and localized modes in the learned distribution. These regions of sharpness are indicative of isolated points in the learned density, which can be effectively identified and quantified through the eigenvalues of the Hessian of the log probability. Large negative eigenvalues reflect sharp peaks, providing a geometric signal of memorization.

While memorization may arise from various factors, our focus is not on analyzing these causes but rather on detecting and understanding the phenomenon itself. By concentrating on the sharpness of the learned density, our framework provides a consistent and practical approach to identifying memorization in diffusion models.

Lastly, we note that this analysis applies to both conditional and non-conditional probability landscapes, depending on the context of the diffusion model’s task or application.

4.2 Detecting Memorization via Hessian Analysis

We propose that the eigenvalues of the Hessian are a key feature for understanding and detecting memorization in diffusion models. Specifically, we introduce a novel metric: counting the strictly positive eigenvalues of the Hessian to capture the degree of memorization. This metric effectively measures the local intrinsic dimension of the probability manifold Ross et al. [2024], offering a geometric perspective on how memorization manifests in the learned distribution.

When memorization occurs, the learned density of the model exhibits sharp, localized peaks around specific samples. This sharpness can be effectively identified using the Hessian, which represents the second derivative of the log probability density (or equivalently, the first derivative of the score function). Intuitively, if most eigenvalues of the Hessian are significantly negative, it indicates that the sample resides at an isolated peak—an unmistakable geometric signal of memorization. Conversely, a higher count of positive eigenvalues suggests that the sample lies on a smoother, higher-dimensional surface of the learned distribution, allowing for variation in multiple directions, which is characteristic of generalized samples.

One significant advantage of analyzing the Hessian is its ability to detect memorization at specific data points at any timestep, even at the earliest stages of the sampling process. Our experiments reveal that Hessian eigenvalues differ notably from the very beginning between cases where memorization occurs and those where it does not. Furthermore, memorization is not limited to the exact reproduction of training data (Matching Verbatim, MV) but also includes replication of broader features, such as backgrounds or artistic styles present in the training data (Template Verbatim, TV) [Webster, 2023]. The eigenvalues of the Hessian vary with the degree of memorization, effectively capturing changes in the local intrinsic dimension of the probability manifold in these cases.

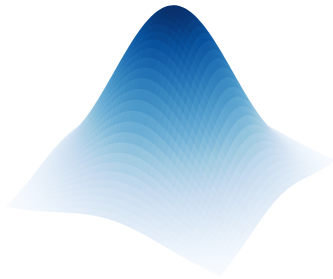
These findings strongly support our hypothesis that the Hessian eigenvalues serve as a robust geometric indicator of memorization, providing both theoretical insights and practical tools for detecting and quantifying memorization in diffusion models.

5 Experiments

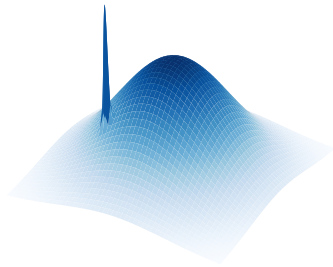
In this section, we investigate deeper into the memorization phenomenon observed in diffusion models trained on various scale of datasets, utilizing our geometric framework for analysis. Specifically, we examine the Hessian eigenvalues (i.e., the Jacobian of the learned score) across the sampling path of the generated samples.

5.1 Memorization in a simple Gaussian

As an illustrative example, we first analyze the memorization phenomenon in a two-dimensional setting. The true density is defined as a simple Gaussian, with an additional single point located far from the Gaussian distribution. Specifically, we sample 3,000 points from the Gaussian density and duplicate the distant point 100 times. This setup is

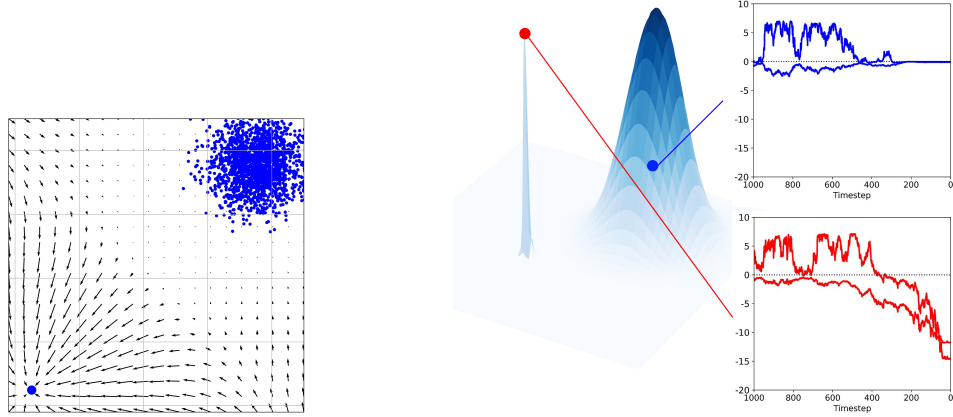


(a) Smooth learned probability landscape



(b) Learned probability landscape with sharp region (memorization)

Figure 1: Illustrative examples of learned probability landscape from diffusion model.



(a) Learned scores and 3,100 training data colored in blue. (b) Eigenvalues for each timestep in memorized and non-memorized samples.

Figure 2: Toy example of a 2D Gaussian mixture with one mode containing 3,000 dispersed points and another mode with 100 highly concentrated points.

designed to induce strong memorization at the duplicated point while maintaining a well-generalized region within the Gaussian distribution, where no memorization is expected. By constructing this contrast, we aim to compare the curvature of sampling path between the memorized and generalized regions.

After training a diffusion model, we generate 5,000 samples. As expected, no signs of memorization appear for samples on the Gaussian surface, while strong memorization is evident at the duplicated data point. Furthermore, as shown in Figure 2a, the learned scores around the duplicated point exhibit greater magnitudes, strongly pulling the sample paths toward the memorized point.

To further analyze, we select one sample each from the memorized and non-memorized regions. We compute the Hessian, $H(\mathbf{x}_t, t)$, for both samples across all 1,000 timesteps, as illustrated in Figure 2b. As expected, near timestep 0, the eigenvalues of $H(\mathbf{x}_t, t)$ for the memorized sample drop to negative values, indicating a sharp curvature. In contrast, the eigenvalues for the non-memorized sample has eigenvalues both near zero, indicating locally smoother region.

5.2 Memorization in MNIST

We further explore memorization in the MNIST dataset, which resides in a 784-dimensional space. To directly examine the geometric behavior of memorized and non-memorized samples, we deliberately assign specific classes to induce memorization, thereby constructing distinct conditional densities.

Specifically, we designate digits 3 and 9 as the non-memorized and memorized classes, respectively. For digit 3, we randomly select 3,000 unique images to represent the non-memorized class. Conversely, for digit 9, we select a single image and duplicate it 30 times to induce strong memorization within the model, similar to the two-dimensional setup. Using this modified dataset of 3,030 samples, we train a DDPM with a second-order loss to ensure accurate computation of the Hessian.

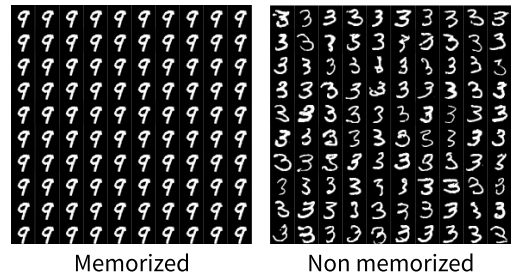


Figure 3: Generated samples of memorized (digit 9), and non-memorized (digit 3) classes.

As depicted in Figure 3, the model generates a wide variety of shapes for digit 3, indicating its ability to generalize effectively. In contrast, for digit 9, the model exclusively reproduces the single duplicated image, confirming that it has fully memorized this specific instance.

For analysis, we generate 10,000 samples for digit 3 using a DDIM sampler with 1,000 steps and compare each generated sample against the entire training set using calibrated ℓ_2 distance [Carlini et al., 2023]. From this comparison, we identify 2,000 samples that are clearly distinguishable from the training set and can reliably be considered free from memorization. For digit 9, we directly generate 2,000 samples, as the model consistently reproduces the memorized

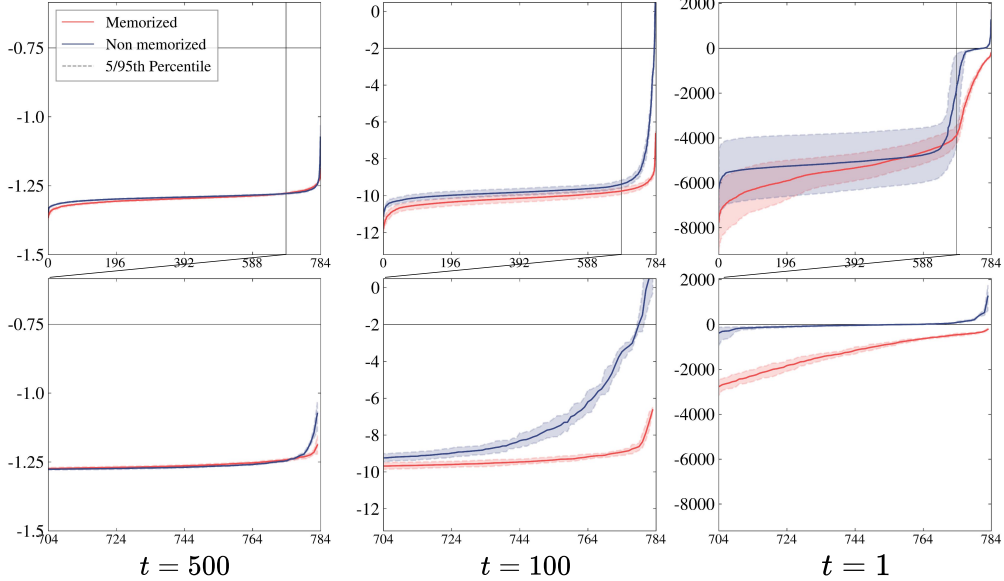


Figure 4: Sorted Hessian eigenvalues for 2,000 memorized and non-memorized samples at selected timesteps (Top), with a zoomed-in view of the top 80 eigenvalues (Bottom).

image. We then compute the eigenvalues of the Hessian, $H(\mathbf{x}_t, t, digit)$, for a total of 4,000 samples across all sampling steps. Analysis at $t = 0$ is omitted due to the divergence of scores as $t \rightarrow 0$.

In Figure 4, we present the sorted 784 eigenvalues for selected timesteps. As t approaches 0, the overall magnitudes of the eigenvalues increase significantly. For instance, at $t = 500$, all eigenvalues are near 0, whereas at $t = 1$, some eigenvalues reach approximately -9,000. This behavior aligns with the denoising process in DMs, where $p_t(\mathbf{x}_t)$ transitions from the prior distribution $\mathcal{N}(\mathbf{0}, \mathbf{I})$ to the target distribution $p(\mathbf{x})$. Thus, the sampling path sharpens progressively, reflecting the increasing concentration of the density, regardless of whether the sample is memorized.

Focusing on $t = 1$, where $p_1(\mathbf{x}_1 | digit) \approx p(\mathbf{x} | digit)$, we identify two key observations. First, for memorized digits, all eigenvalues are negative, indicating that the sample resides at the peak of an isolated, sharp curvature. In contrast, non-memorized samples exhibit some positive eigenvalues, suggesting they lie along the edges of the surface, where remaining directions allow for movement. We illustrate how the number of positive eigenvalues changes over timesteps in Figure 5. After a certain timestep, non-memorized samples consistently remain along edges with available directions to explore, while memorized samples remain fixed on concave surfaces, unable to ascend further.

Another notable point is that, although positive eigenvalues exist for non-memorized samples, their number is limited to approximately 24. This observation aligns with findings by Pope et al. [2021], where the intrinsic dimensionality of the latent manifold of image data is shown to be significantly smaller than the full image dimensionality. Consequently, while non-memorized samples span most of the manifold surface, this can be reflected by a much smaller proportion of positive eigenvalues compared to the negative ones. We leave the exploration of Hessian eigenvalue analysis as a tool to examine the latent dimensionality of data for future work.

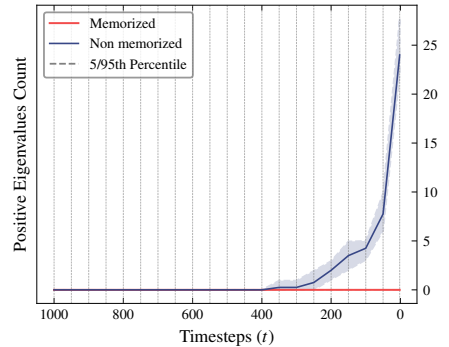


Figure 5: Number of positive eigenvalues of the Hessian for 2,000 memorized and non-memorized samples every 50 timesteps.

5.3 Memorization in Stable Diffusion

From the previous experiments, we consistently observe that memorized samples reside on sharp surfaces, as indicated by the Hessian eigenvalues, whereas non-memorized samples do not exhibit this behavior. Here, we extend this analysis to explain the phenomenon at the scale of Stable Diffusion [Rombach et al., 2022].

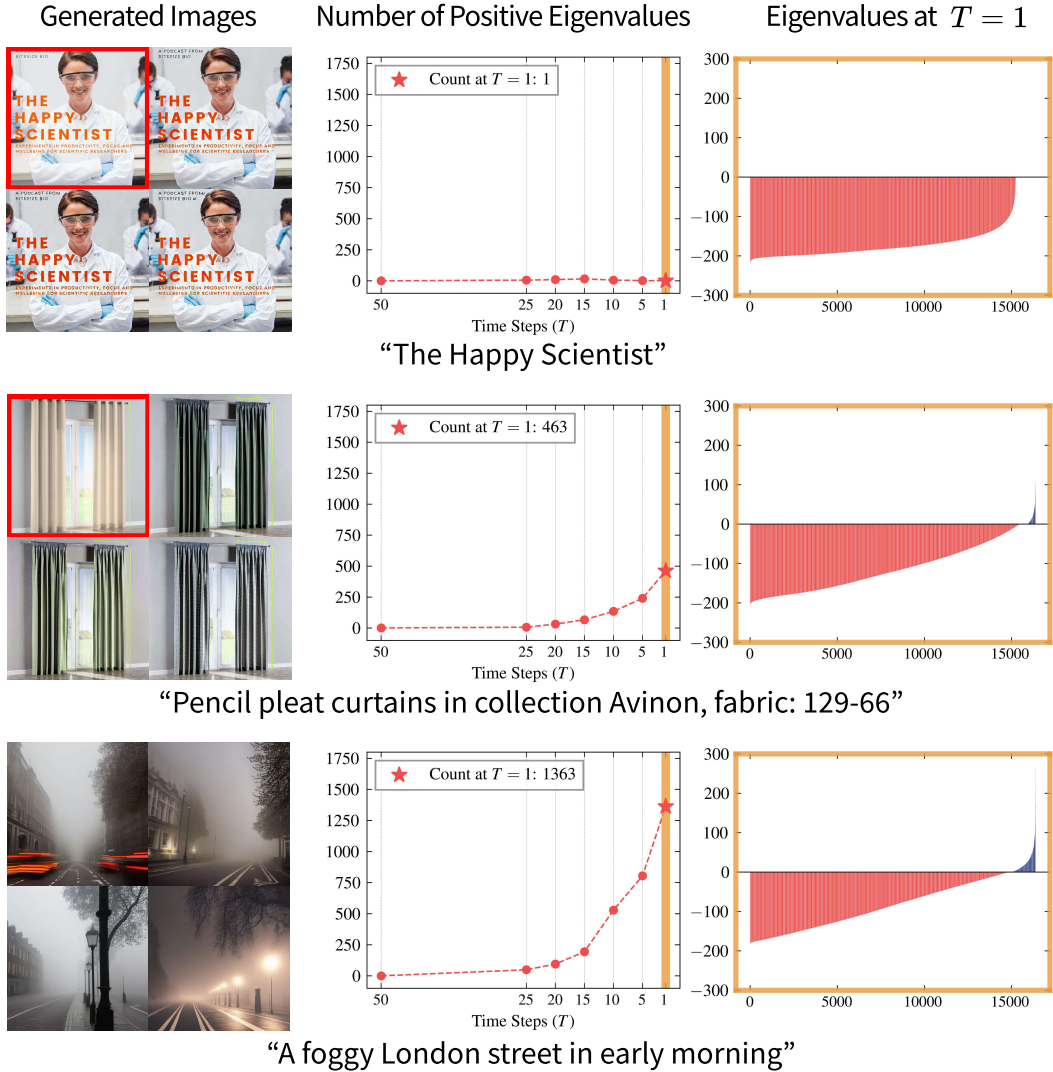
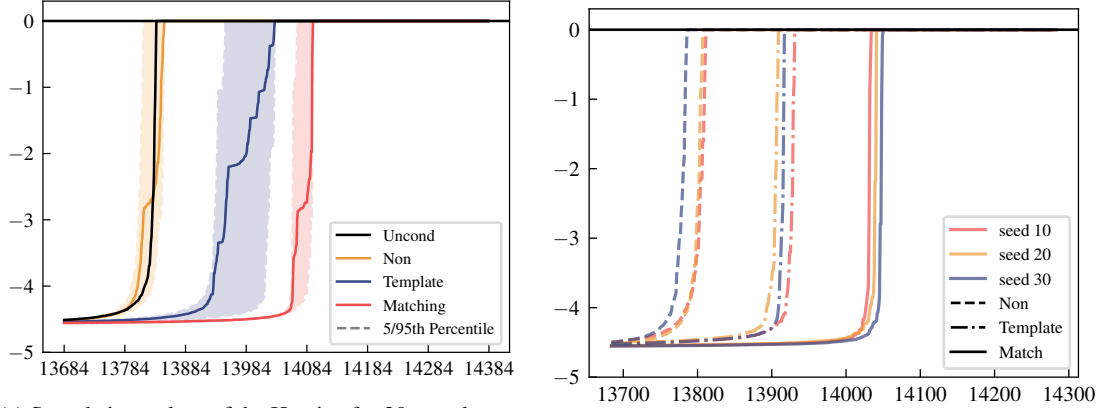


Figure 6: Hessian eigenvalue analysis for three different samples corresponding to each verbatim category (Matching, Template, None) shown in rows. Images outlined in red represent training data from Stable Diffusion v1, while the others are generated by the model.

Experiment Setup. For our experiment, we use Stable Diffusion v1.4 and focus on memorized prompts identified in Webster [2023], where the SSCD score [Pizzi et al., 2022] between the memorized and generated images exceeds 0.7. We use two types of verbatims from the categories defined by Webster [2023]. The first is matching verbatim, where the generated images are an exact pixel-by-pixel match with the original paired training image. The second is template verbatim, where the generated images partially resemble the training image, with variations in colors or styles. Additionally, we include non-memorized prompts from Ren et al. [2024], referred to as non-verbatims, which are generated using ChatGPT-4 [Achiam et al., 2023].

As Stable Diffusion operates in a high-dimensional space of 16,384 dimensions, directly calculating eigenvalues using the explicit Hessian incurs significant computational costs. To address this, we employ Arnoldi iteration, which allows eigenvalue computation without explicitly forming the Hessian. We leverage `torch.autograd.functional.jvp` to efficiently perform the calculations within the model. Refer to Section 3 for more details.

Categorizing Verbatims through Curvature. From a geometric perspective, we expect matching verbatims to reside at isolated peaks, as these samples exhibit minimal variation, with nearly every pixel identical to the memorized training image. In contrast, template verbatims are positioned near peaks but are less sharp due to their ability to accommodate variations such as colors or styles. Non-verbatims, on the other hand, are expected to lie along the edges of smoother regions, allowing for multiple directions of movement.



(a) Sorted eigenvalues of the Hessian for 30 samples per verbatim and the unconditional case at the early sampling stage. The range is clipped, showing 900/16,384.

(b) Sorted eigenvalues at the early sampling stage for a fixed prompt set. The range is clipped, showing 600/16,384.

Figure 7: Identifying Verbatims at the Early Sampling Stages

After generating samples from each verbatim using the DDIM sampler (50 steps in total), we present the fully sorted eigenvalues for each verbatim category in Figure 6. As expected, the number of positive eigenvalues increases gradually from matching verbatim to non-verbatim (see the last column), intuitively illustrating that the variability in possible directions grows as we move onto non-verbatim. Additionally, while the number of positive eigenvalues gradually increases for template and non-verbatim samples as t approaches 0, matching verbatim samples consistently remain on concave surfaces (see the middle column), aligning with the observations from the MNIST experiments. To ensure numerical stability during interpretation, we exclude near-zero eigenvalues below 1×10^{-15} when counting the number of positive eigenvalues. Additional figures for more samples are provided in Appendix A.

Identifying Verbatims at the Early Sampling Stages If a certain density is significantly sharper than others, it will remain sharper even after numerous random noises are added. Building on our observation that memorized samples reside at sharp peaks, we investigate whether this curvature difference among verbatims is already detectable at the early stage of sampling.

To examine this, we select a single $\mathbf{z} \sim \mathcal{N}(\mathbf{0}, \mathbf{I})$ and randomly sample 30 prompts from each verbatim category. We then calculate the Hessian eigenvalues in the initial sampling stage, as illustrated in Figure 7a. Interestingly, memorized prompts exhibit a significantly larger number of negative eigenvalues, while also showing a clear distinction between template and matching verbatims. Template verbatims, in particular, exhibit greater deviations, reflecting varying degrees of memorization across prompts, such as differences in color or style. In contrast, non-verbatim samples behave similarly to the unconditional case, where no prompt is provided, indicating that these prompts yield conditional densities that closely align with the marginal density, showing minimal differences.

To confirm whether the differences among verbatim categories persist across different initializations, we analyze the eigenvalues for three fixed prompts from each category with varying starting points. As shown in Figure 7b, the results remain consistent in three different initializations of \mathbf{z} . These empirical findings demonstrate that verbatim categories can be reliably distinguished using Hessian eigenvalues, even at the initial timestep.

6 Conclusion and Future works

Our study provides empirical evidence that the phenomenon of memorization in diffusion models can be effectively understood through a simple geometric framework: the sharpness of the density curvature. By analyzing Hessian eigenvalues, we systematically investigate and explain the differences in density curvature between memorized and non-memorized samples, ranging from toy datasets to large-scale models like Stable Diffusion.

For future work, we aim to conduct a more rigorous analysis of how conditioning via embeddings like CLIP encoder [Radford et al., 2021] alters the distribution, offering deeper insights into the behavior of memorized data in large generative models. Additionally, developing effective mitigation strategies based on our findings represents a promising research direction. Given that our method can detect memorization at an early stage, it could be utilized to design proactive approaches for mitigating memorization. Furthermore, extending our analysis to one-step models, such as rectified flow [Liu et al., 2023], could pave the way for novel designs of sampling ODE trajectories.

References

- J. Achiam, S. Adler, S. Agarwal, L. Ahmad, I. Akkaya, F. L. Aleman, D. Almeida, J. Altenschmidt, S. Altman, S. Anadkat, et al. Gpt-4 technical report. *arXiv preprint arXiv:2303.08774*, 2023.
- A. Alakhdar, B. Poczos, and N. Washburn. Diffusion models in de novo drug design. *Journal of Chemical Information and Modeling*, 2024.
- W. E. Arnoldi. The principle of minimized iterations in the solution of the matrix eigenvalue problem. *Quarterly of Applied Mathematics*, 1951.
- R. Bhattacharjee, S. Dasgupta, and K. Chaudhuri. Data-copying in generative models: a formal framework. In *International Conference on Machine Learning*, 2023.
- G. Biroli, T. Bonnaire, V. De Bortoli, and M. Mézard. Dynamical regimes of diffusion models. *Nature Communications*, 2024.
- T. Brooks, J. Hellsten, M. Aittala, T.-C. Wang, T. Aila, J. Lehtinen, M.-Y. Liu, A. Efros, and T. Karras. Generating long videos of dynamic scenes. In *NeurIPS*, 2022.
- N. Carlini, J. Hayes, M. Nasr, M. Jagielski, V. Sehwag, F. Tramèr, B. Balle, D. Ippolito, and E. Wallace. Extracting training data from diffusion models. In *USENIX Security*, 2023.
- M. Caron, H. Touvron, I. Misra, H. Jégou, J. Mairal, P. Bojanowski, and A. Joulin. Emerging properties in self-supervised vision transformers. In *CVPR*, 2021.
- C. Chen, D. Liu, M. Shah, and C. Xu. Exploring local memorization in diffusion models via bright ending attention. *arXiv preprint arXiv:2410.21665*, 2024.
- A. Das. Building diffusion model’s theory from ground up. In *ICLR Blogposts 2024*, 2024.
- C. Fefferman, S. Mitter, and H. Narayanan. Testing the manifold hypothesis. *Journal of the American Mathematical Society*, 2016.
- X. Gu, C. Du, T. Pang, C. Li, M. Lin, and Y. Wang. On memorization in diffusion models. *arXiv preprint arXiv:2310.02664*, 2023.
- J. Ho, A. Jain, and P. Abbeel. Denoising diffusion probabilistic models. In *NeurIPS*, 2020.
- J. Ho, T. Salimans, A. Gritsenko, W. Chan, M. Norouzi, and D. J. Fleet. Video diffusion models. In *NeurIPS*, 2022.
- C. Horvat and J.-P. Pfister. On gauge freedom, conservativity and intrinsic dimensionality estimation in diffusion models. In *ICLR*, 2024.
- B. M. Joseph Saveri. Stable diffusion litigation, 2023. URL <https://stablediffusionlitigation.com/>.
- Z. Kadkhodaie, F. Guth, E. P. Simoncelli, and S. Mallat. Generalization in diffusion models arises from geometry-adaptive harmonic representations. In *ICLR*, 2024.
- H. Kamkari, B. L. Ross, R. Hosseinzadeh, J. C. Cresswell, and G. Loaiza-Ganem. A geometric view of data complexity: Efficient local intrinsic dimension estimation with diffusion models. In *ICML 2024 Workshop on Structured Probabilistic Inference & Generative Modeling*, 2024.
- C. Lanczos. An iteration method for the solution of the eigenvalue problem of linear differential and integral operators. *J. Res. Natl. Bur. Stand. B*, 1950.
- X. Liu, C. Gong, and qiang liu. Flow straight and fast: Learning to generate and transfer data with rectified flow. In *ICLR*, 2023.
- C. Lu, K. Zheng, F. Bao, J. Chen, C. Li, and J. Zhu. Maximum likelihood training for score-based diffusion odes by high order denoising score matching. In *ICML*, 2022.
- C. Meng, Y. Song, W. Li, and S. Ermon. Estimating high order gradients of the data distribution by denoising. In *NeurIPS*, 2021.
- W. H. Orrick. Andersen v. Stability AI Ltd., 2023. URL <https://casetext.com/case/andersen-v-stability-ai-ltd>.
- J. Pidstrigach. Score-based generative models detect manifolds. In *NeurIPS*, 2022.
- E. Pizzi, S. D. Roy, S. N. Ravindra, P. Goyal, and M. Douze. A self-supervised descriptor for image copy detection. In *CVPR*, 2022.
- D. Podell, Z. English, K. Lacey, A. Blattmann, T. Dockhorn, J. Müller, J. Penna, and R. Rombach. SDXL: Improving latent diffusion models for high-resolution image synthesis. In *ICLR*, 2024.

- P. Pope, C. Zhu, A. Abdelkader, M. Goldblum, and T. Goldstein. The intrinsic dimension of images and its impact on learning. In *ICLR*, 2021.
- A. Radford, J. W. Kim, C. Hallacy, A. Ramesh, G. Goh, S. Agarwal, G. Sastry, A. Askell, P. Mishkin, J. Clark, G. Krueger, and I. Sutskever. Learning transferable visual models from natural language supervision. In *ICML*, 2021.
- J. Ren, Y. Li, S. Zeng, H. Xu, L. Lyu, Y. Xing, and J. Tang. Unveiling and mitigating memorization in text-to-image diffusion models through cross attention. In *ECCV*, 2024.
- R. Rombach, A. Blattmann, D. Lorenz, P. Esser, and B. Ommer. High-resolution image synthesis with latent diffusion models. In *CVPR*, 2022.
- B. L. Ross, H. Kamkari, T. Wu, R. Hosseinzadeh, Z. Liu, G. Stein, J. C. Cresswell, and G. Loaiza-Ganem. A geometric framework for understanding memorization in generative models. *arXiv preprint arXiv:2411.00113*, 2024.
- C. Saharia, W. Chan, S. Saxena, L. Li, J. Whang, E. L. Denton, K. Ghasemipour, R. Gontijo Lopes, B. Karagol Ayan, T. Salimans, et al. Photorealistic text-to-image diffusion models with deep language understanding. In *NeurIPS*, 2022.
- G. Somepalli, V. Singla, M. Goldblum, J. Geiping, and T. Goldstein. Diffusion art or digital forgery? investigating data replication in diffusion models. In *CVPR*, 2023a.
- G. Somepalli, V. Singla, M. Goldblum, J. Geiping, and T. Goldstein. Understanding and mitigating copying in diffusion models. In *NeurIPS*, 2023b.
- J. Song, C. Meng, and S. Ermon. Denoising diffusion implicit models. In *ICLR*, 2021a.
- Y. Song, C. Durkan, I. Murray, and S. Ermon. Maximum likelihood training of score-based diffusion models. In *NeurIPS*, 2021b.
- Y. Song, J. Sohl-Dickstein, D. P. Kingma, A. Kumar, S. Ermon, and B. Poole. Score-based generative modeling through stochastic differential equations. In *ICLR*, 2021c.
- J. Stanczuk, G. Batzolis, T. Deveney, and C.-B. Schönlieb. Diffusion models encode the intrinsic dimension of data manifolds. In *ICML*, 2024.
- G. Stein, J. C. Cresswell, R. Hosseinzadeh, Y. Sui, B. L. Ross, V. Vilecroze, Z. Liu, A. L. Caterini, E. Taylor, and G. Loaiza-Ganem. Exposing flaws of generative model evaluation metrics and their unfair treatment of diffusion models. In *NeurIPS*, 2023.
- P. Tempczyk, R. Michaluk, L. Garncarek, P. Spurek, J. Tabor, and A. Golinski. Lidl: Local intrinsic dimension estimation using approximate likelihood. In *ICML*, 2022.
- H. Touvron, T. Lavril, G. Izacard, X. Martinet, M.-A. Lachaux, T. Lacroix, B. Rozière, N. Goyal, E. Hambro, F. Azhar, et al. Llama: Open and efficient foundation language models. *arXiv preprint arXiv:2302.13971*, 2023.
- E. Ventura, B. Achilli, G. Silvestri, C. Lucibello, and L. Ambrogioni. Manifolds, random matrices and spectral gaps: The geometric phases of generative diffusion. *arXiv preprint arXiv:2410.05898*, 2024.
- R. Webster. A reproducible extraction of training images from diffusion models. *arXiv preprint arXiv:2305.08694*, 2023.
- Y. Wen, Y. Liu, C. Chen, and L. Lyu. Detecting, explaining, and mitigating memorization in diffusion models. In *ICLR*, 2024.
- L. K. Wenliang and B. Moran. Score-based generative models learn manifold-like structures with constrained mixing. In *NeurIPS Workshop SBM*, 2023.
- M. Yi, J. Sun, and Z. Li. On the generalization of diffusion model. *arXiv preprint arXiv:2305.14712*, 2023.
- T. Yoon, J. Y. Choi, S. Kwon, and E. K. Ryu. Diffusion probabilistic models generalize when they fail to memorize. In *ICML 2023 Workshop on Structured Probabilistic Inference & Generative Modeling*, 2023.

A Additional Results for Stable Diffusion

In Figure 8, Figure 9, and Figure 10, we provide additional results of eigenvalue analysis for different prompts at timestep 1.

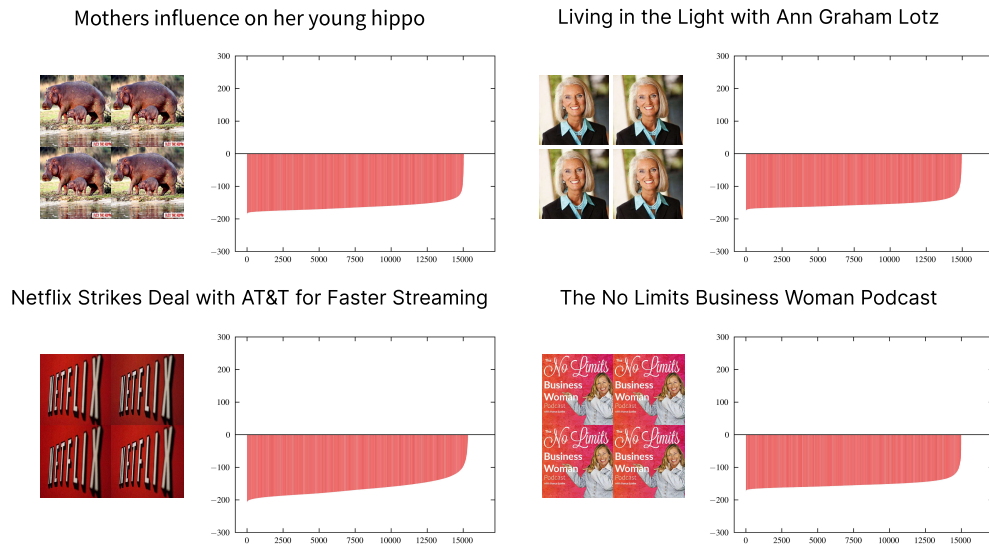


Figure 8: Matching verbatims, and their corresponding eigenvalues at timestep 1.

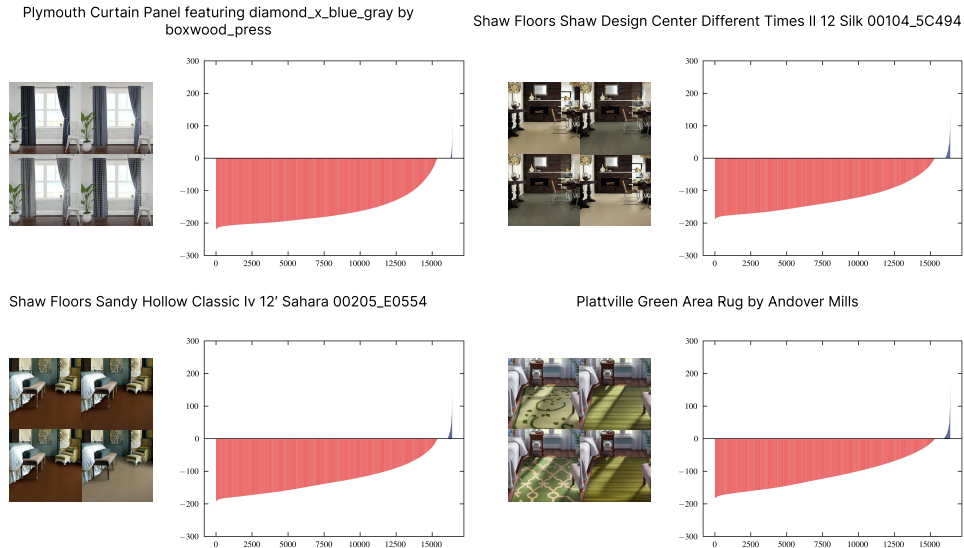


Figure 9: Template verbatims, and their corresponding eigenvalues at timestep 1.

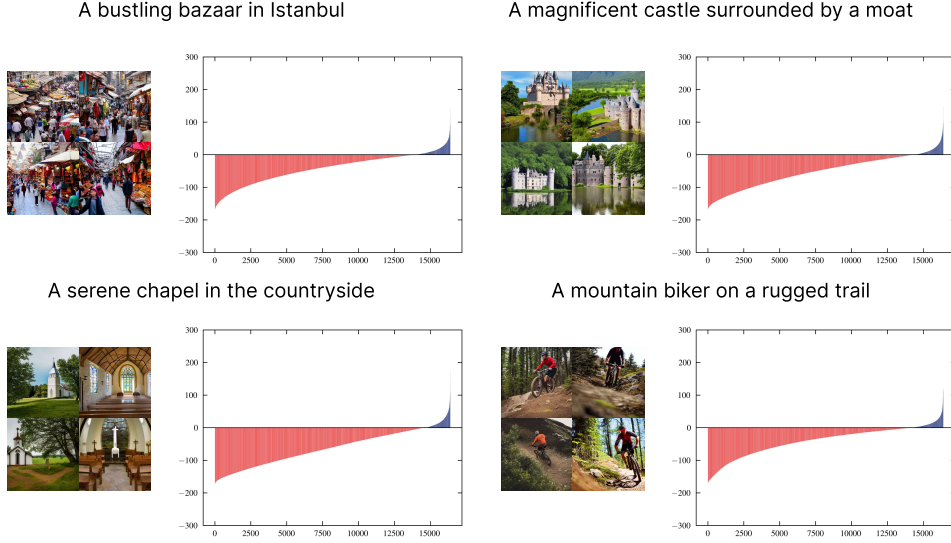


Figure 10: Non-verbatims, and their corresponding eigenvalues at timestep 1.

B Arnoldi Iteration

Algorithm 1 Arnoldi Iteration using Jacobian-Vector Products

Require: Starting vector $\mathbf{b} \in \mathbb{R}^d$, number of iterations $m < d$, function $\text{jvp_func}(\mathbf{v})$ that computes $\mathbf{A}\mathbf{v}$, threshold ε

Ensure: Orthonormal basis $\mathbf{Q}_m = [\mathbf{q}_1, \dots, \mathbf{q}_m]$, upper Hessenberg matrix $\mathbf{H}_m \in \mathbb{R}^{m \times m}$

- 1: Initialize $\mathbf{Q} \in \mathbb{R}^{d \times (m+1)}$, $\mathbf{h} \in \mathbb{R}^{(m+1) \times m}$
 - 2: Normalize the starting vector: $\mathbf{q}_1 = \frac{\mathbf{b}}{\|\mathbf{b}\|_2}$
 - 3: **for** $k = 1$ to m **do**
 - 4: Compute $\mathbf{v} = \text{jvp_func}(\mathbf{q}_k)$
 - 5: **for** $j = 1$ to k **do**
 - 6: Compute $h_{j,k} = \mathbf{q}_j^\top \mathbf{v}$
 - 7: Update $\mathbf{v} = \mathbf{v} - h_{j,k} \mathbf{q}_j$
 - 8: **end for**
 - 9: Compute $h_{k+1,k} = \|\mathbf{v}\|_2$
 - 10: **if** $h_{k+1,k} > \varepsilon$ **then**
 - 11: Normalize $\mathbf{q}_{k+1} = \frac{\mathbf{v}}{h_{k+1,k}}$
 - 12: **else**
 - 13: **Terminate iteration**
 - 14: **end if**
 - 15: **end for**
 - 16: Adjust \mathbf{H}_m by removing the last row of \mathbf{h}
 - 17: **return** $\mathbf{Q}_m = [\mathbf{q}_1, \dots, \mathbf{q}_m]$, $\mathbf{H}_m = [h_{i,j}]_{i=1,\dots,m; j=1,\dots,m}$
-